

A computational framework for simulation of the delivery of substances into cells

Eduardo M. B. Campello^{1,2,*†} and Tarek I. Zohdi²

¹*Department of Structural and Geotechnical Engineering, Polytechnic School, University of São Paulo, P.O. Box 61548, 05424-970, São Paulo, SP, Brazil*

²*Department of Mechanical Engineering, University of California at Berkeley, 6195 Etcheverry Hall, 94720-1740, Berkeley, CA, USA*

SUMMARY

In this paper, we propose a simple computational framework for the rapid simulation of the delivery of substances into cells. Our approach treats the substances and the cell membrane as a collection of particles forming a discrete dynamical system, which is described by Newtonian equations in a purely mechanistic way. Detailed aspects about the modeling of particle interactions are discussed and resolved. The main advantage of such an approach is that it can offer a good qualitative picture of the delivery mechanism without the need to resort to detailed descriptions of the complex intermolecular interactions that are observed at small scales of the cell membrane. A numerical time integration scheme is formulated for solution of the system dynamics, and examples of simulations are provided. Computational particle-based models render reliable and fast simulation tools. We believe they can be very useful to help advance the design of delivery systems. Copyright © 2014 John Wiley & Sons, Ltd.

Received 04 December 2013; Revised 17 March 2014; Accepted 10 April 2014

KEY WORDS: cells; cell membranes; drug delivery; micro projectiles; particle methods; discrete element methods

1. INTRODUCTION AND PROBLEM DEFINITION

The delivery of substances into cells is an important tool in modern cell biology. Drugs, proteins (antibodies or enzymes), genetic material (RNA or DNA), biological stains, and many other materials are often desired to be transported to the interior of the cells to undertake a specific task. The cell membrane constitutes the main physical barrier in this regard (in the case of plant cells, there is also the cell wall). Some of the existing technologies to accomplish such transport include uptake mechanisms, fusion mechanisms, use of infectious agents, use of micro-injection and nano-injection devices, and particle bombardment guns. None of these, however, is free from disadvantages or limitations.

In recent years, technologies involving particle bombardment guns (also commonly referred to as biolistic or bioballistic systems), whose shots consist of either single particles or jets of particles, have been preferred in many applications. This is partly due to their ability to deal with (i) cells both *in vitro* and *in vivo*, that is, cells either in suspension or in their natural environment, and (ii) groups of cells simultaneously, instead of only single cells at a time. Particle guns were first introduced in [1, 2] when dealing with epidermal onion cells and rely on a very simple principle: if the incoming particles have the appropriate size and are accelerated to the appropriate velocities, they should

*Correspondence to: Eduardo M. B. Campello, Department of Mechanical Engineering, University of California at Berkeley, 6195 Etcheverry Hall, Berkeley, CA, 94720-1740, USA.

†E-mail: campello@usp.br

readily penetrate thin barriers such as cell walls and cell membranes, thereby entering the cell cytoplasm. The idea is schematically illustrated in Figure 1, where typical dimensions are also shown.

One important aspect to consider in bombardment systems is the lipid bilayer structure of the cell membrane and its underlying molecular arrangement. In general, lipid molecules are idealized as spherical polar heads (representing a phosphoric group) having one or two elongated tails (representing hydrocarbon, fatty acid chains). In aqueous media, as it is well known, they organize themselves into various types of structures due to their amphiphilic property (the polar heads are hydrophilic, the hydrocarbon chains are hydrophobic), one of which is the two-layer formation that is observed in cellular membranes. The forces that hold these molecules together in such a configuration are not due to strong covalent or ionic bonds but instead arise from weaker van der Waals, hydrophobic, and hydrogen-bonding interactions. This provides the membrane a very soft, flexible, almost fluid-like, behavior, and yet, good response to both stretching and bending deformations, along with excellent selective permeability, is observed. The transport of substances across the membrane barrier by means of particle bombardment is greatly governed by the mechanical characteristics of this structure.

In this context, the purpose of this work is to present a relatively simple, yet relatively robust, computational framework for the simulation of particle-gun delivery systems. It can be numerically implemented with small effort by researchers interested in the field and can be easily tailored to many specific applications. We follow a purely mechanistic description (in the sense that biological and chemical aspects present in the transport phenomenon are not directly addressed), keeping our focus only on the mechanical forces that dictate the response of the problem. Both the cell membrane and the incoming substances are treated as a collection of spherical particles forming a discrete dynamical system, in which each particle interacts with the others and the surrounding media via a complex combination of bonding forces, fluid pressure, drag, and contact and friction forces due to touching and collisions. Classical Newtonian dynamics is adopted to describe the time evolution of the system, the equations of which are solved via a numerical (time-stepping) integration scheme. Examples of numerical simulations are provided to show how the model works from a general perspective. We remark that it is not our intention here to perform thorough assessment of the model's parameters and obtained results but instead just to present the general framework that we have devised and show how it may be applied to the simulation of particle bombardment mechanisms. Detailed calibration of parameters and validation against results from physical experiments are left as a matter of further research, which is currently being conducted by the authors and will be presented in a forthcoming paper.

The proposed approach falls in the class of particle-based methods or discrete element methods, see, for example, [3–5]. There exists a number of other theoretical and/or computational approaches that may be used to study the transport of substances across the cell membrane, for example, stochastic dynamics [6, 7], Monte Carlo simulations [8, 9], molecular dynamics models [10–12], mean field models [13], and continuum mechanics models with spatial discretizations [14], to name and cite just a few. Yet, at the tens of nano-time to a few micro-time and length scales, we believe that particle-based models are the most suited when one is interested in the overall (collective), qualitative behavior of the system. They allow for a simple representation of the whole cell and incoming substances. Also, multiple contact/impact with the opening of localized holes on the membrane surface (localized ‘rupture’) is straightforward to characterize. They offer a good picture of the structure and

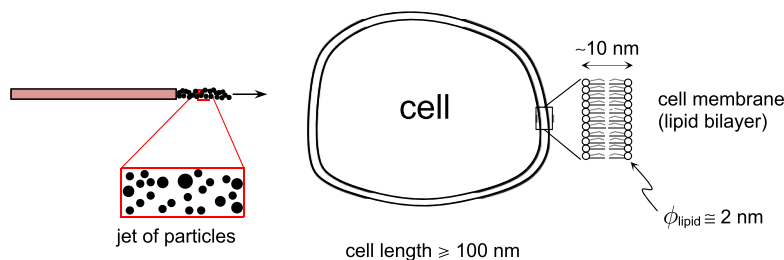


Figure 1. Particle bombardment for the delivery of substances into a cell.

the dynamics of the membrane when hit by particles or jets of particles, without requiring detailed descriptions of the complex short-range forces that act between polar headgroups and hydrocarbon chains of the lipid molecules. They provide the construction of rapid, qualitative simulation tools. With such tools, particle-gun devices can be more thoroughly designed and tested without the need of resorting to a great number of physical experiments. Physical experiments can be expensive and time consuming, and the parameters that can be adjusted within feasible cost and time are very limited when compared to computational investigations.

The paper is organized as follows: in Section 2, we present a brief description of the equations that govern the dynamics of particulate systems (with emphasis on the several types of mechanical forces involved herein and their possible representations); in Section 3, we explain how we model the cell membrane and the bonding forces between its lipid particles (this was performed separately from Section 2 such that specific aspects could be more carefully addressed); in Section 4, we give an overview of our numerical solution scheme to the system's equations; in Section 5, we show examples of numerical simulations that were carried out by varying different geometrical parameters of a model problem; and in Section 6, we conclude the paper with some remarks and ideas for future work.

Throughout the text, plain italic letters ($a, b, \dots, \alpha, \beta, \dots, A, B, \dots$) denote scalar quantities, whereas boldface italic ones ($\mathbf{a}, \mathbf{b}, \dots, \boldsymbol{\alpha}, \boldsymbol{\beta}, \dots, \mathbf{A}, \mathbf{B}, \dots$) denote vectors in a three-dimensional Euclidean space. The inner product of two vectors is denoted by

$$\mathbf{u} \cdot \mathbf{v} = u_1 v_1 + u_2 v_2 + u_3 v_3, \quad (1)$$

where u_i and v_i ($i = 1, 2, 3$) are the corresponding three components of the vectors, and the norm of a vector by

$$\|\mathbf{u}\| = \sqrt{\mathbf{u} \cdot \mathbf{u}} = \sqrt{u_1^2 + u_2^2 + u_3^2}. \quad (2)$$

2. DYNAMICS OF PARTICULATE SYSTEMS

We assume at the outset that the particles are spherical and that they are small enough so that the effect of their rotations with respect to their center of mass is unimportant to their overall motion. Moreover, permanent deformations due to contact and collisions are supposed to be minor and thereby ignored, which means that all particles remain spherical and with constant radius at all times. Effects of temperature changes are also considered to be irrelevant—although these can be easily incorporated, following, for example, the scheme proposed in [15].

Let our system be comprised of N_p particles, each one with known mass m_i and known radius R_i . We denote the position vector of particle i by \mathbf{r}_i , the velocity vector by \mathbf{v}_i , and the acceleration vector by \mathbf{a}_i . According to Newton's second law, at every time instant t , the following equation must hold for each particle:

$$m_i \mathbf{a}_i = \mathbf{f}_i^{tot}, \quad (3)$$

where \mathbf{f}_i^{tot} is the total force vector acting on the particle. This vector is made up of the sum of four force contributions as follows:

$$\mathbf{f}_i^{tot} = \mathbf{f}_i^{env} + \mathbf{f}_i^{bond} + \mathbf{f}_i^{con} + \mathbf{f}_i^{fric}, \quad (4)$$

in which \mathbf{f}_i^{env} comprises the forces due to the environment acting on the particle (they represent the effects of the surrounding media on the particle), \mathbf{f}_i^{bond} comprises the forces due to bonding or adhesive interactions with other particles, \mathbf{f}_i^{con} comprises the forces due to mechanical contact (or collisions)

with other particles and/or obstacles, and \mathbf{f}_i^{fric} comprises the forces due to friction that arise from these contacts or collisions.

For the forces due to the environment, we write

$$\mathbf{f}_i^{env} = m_i \mathbf{g} + \mathbf{f}_i^{pres} + \mathbf{f}_i^{drag} \quad , \quad (5)$$

where \mathbf{g} is the external (i.e., environmental) gravity field, and \mathbf{f}_i^{pres} and \mathbf{f}_i^{drag} are the pressure and drag forces due to the surrounding fluid. The pressure force is a given value or follows a given distribution, whereas the drag force is usually dependent on the particle's velocity (several expressions are possible depending on the characteristics of the flow, see, for example, [16]). Here, we adopt the following simple model, which constitutes a source of damping for the system:

$$\mathbf{f}_i^{drag} = -c_{env}(\mathbf{v}_i - \mathbf{v}_{env}) \quad , \quad (6)$$

in which c_{env} is a damping parameter and \mathbf{v}_{env} is the (local) velocity of the surrounding fluid. This is a one-way kind of coupling between the fluid and the particle, in the sense that the fluid affects the particle but the particle does not affect the fluid. More elaborate, fully coupled models can be constructed if necessary (although this increases the complexity of the solution scheme, because it introduces the fluid local velocity and pressure fields as additional variables). Other environmental forces may be considered in Equation (5), such as electric forces due to external electric fields and magnetic forces due to external magnetic fields. We will comment briefly on this in Section 6.

For the forces due to bonding or adhesive interactions with other particles, we write

$$\mathbf{f}_i^{bond} = \sum_{j=1}^{N_b} \mathbf{f}_{ij}^{bond} \quad , \quad (7)$$

where N_b is the number of particles that are bonded to particle i and \mathbf{f}_{ij}^{bond} is the (binary) bonding force that acts between particle i and particle j . This force has the general form

$$\mathbf{f}_{ij}^{bond} = K_{ij} \mathbf{n}_{ij} \quad , \quad (8)$$

in which K_{ij} is a scalar quantity dictating the intensity of the bonding for the pair $\{i, j\}$ and \mathbf{n}_{ij} is the unit vector that points from the center of particle i to the center of particle j , that is,

$$\mathbf{n}_{ij} = \frac{\mathbf{r}_j - \mathbf{r}_i}{\|\mathbf{r}_j - \mathbf{r}_i\|} \quad (9)$$

(this vector will be from now on referred to as the pair's central direction). Scalar K_{ij} can be modeled in a number of ways, such as by using a combination of attractive and repulsive force coefficients that are functions of the distance between the particles [15] (this can be understood as derived from a generalized Mie's potential, of which the classical Lennard–Jones potential [17] is a special case), by using surface energy arguments [18, 19], and direct van de Waals effects. In Section 3, we present the model that we have devised for the purpose of this work, which is based on the presence of a fictitious spring-dashpot (SD) connecting particles i and j .

For the forces due to contact and collisions with other particles, there exist two classes of models that may be invoked, namely, the overlap-based model and the impulse-based model. The adoption of one or the other must be dictated by the type of contact/collision that is expected to happen between the particles in the system. The overlap-based model is better suited when the contact involves relatively soft particles and/or situations of enduring contact. In these cases, it is assumed that the contact force is a function of the amount of penetration (i.e., deformation) of the particles in contact, with the overlap between the particles considered as the magnitude of this penetration. This means that the contact deformation has to be resolved and some constitutive equation is thereby

necessary. The assumption of no permanent deformations due to collisions, stated at the beginning of this section, enables us to use the Hertz's elastic contact theory (see [20]) to this end. Accordingly, based on Hertz's solution, here we adopt the following expression for f_i^{con} :

$$f_i^{con} = \sum_{j=1}^{N_c} f_{ij}^{con}, \tag{10}$$

$$f_{ij}^{con} = \frac{4}{3} \sqrt{R^* E^*} \delta^{3/2} \mathbf{n}_{ij} + d \dot{\delta} \mathbf{n}_{ij} \quad (\text{overlap-based model}),$$

where N_c is the number of particles that are in contact with particle i , f_{ij}^{con} is the (binary) contact force that acts between the contacting pair $\{i, j\}$,

$$R^* = \frac{R_i R_j}{R_i + R_j} \quad \text{and} \quad E^* = \frac{E_i E_j}{E_j(1 - \nu_i^2) + E_i(1 - \nu_j^2)} \tag{11}$$

are the effective radius and the effective elasticity modulus of the contacting pair (in which E_i , E_j and ν_i , ν_j are the elasticity modulus and the Poisson coefficient of particles i and j , respectively),

$$\delta = \|\mathbf{r}_i - \mathbf{r}_j\| - (R_i + R_j) \tag{12}$$

is the penetration (or geometric overlap) between the pair in the pair's central direction, $\dot{\delta}$ is the rate of this penetration (the superposed dot denotes differentiation with respect to time), and d is a damping constant that is introduced to allow for some energy dissipation. Figure 2 provides an illustration of a colliding pair.

The impulse-based model, on its turn, is better suited when the contact involves relatively stiff spheres that do not remain in contact after the collision has come to an end. In this case, the collision is an almost instantaneous (i.e., of very small duration) event, and a simple balance of linear momentum before and after it suffices to compute the forces involved. Accordingly, we adopt here the following expression for these cases:

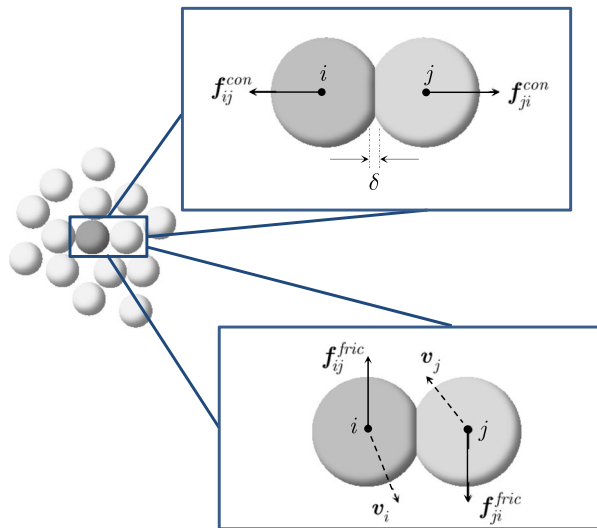


Figure 2. Contact/collision between two particles.

$$\begin{aligned} \mathbf{f}_i^{con} &= \sum_{j=1}^{N_c} \mathbf{f}_{ij}^{con}, \\ \mathbf{f}_{ij}^{con} &= \bar{I}_n \mathbf{n}_{ij} \quad (\text{impulse-based model}), \end{aligned} \tag{13}$$

where \bar{I}_n is the (averaged) impulsive force exerted by the colliding pair over each other in the pair's central direction during the collision, obtained as shown in the APPENDIX and given by

$$\bar{I}_n = \frac{1}{\delta t} \int_{t^*}^{t^* + \delta t} I_n dt = \frac{m_i(v_{in}(t^* + \delta t) - v_{in}(t^*))}{\delta t} - \bar{f}_{in}. \tag{14}$$

Here, t^* is the time instant at the beginning of the collision, δt is the duration of the collision,

$$v_{in}(t^*) = \mathbf{v}_i(t^*) \cdot \mathbf{n}_{ij} \quad \text{and} \quad v_{in}(t^* + \delta t) = \mathbf{v}_i(t^* + \delta t) \cdot \mathbf{n}_{ij} \tag{15}$$

are the components of particle i 's velocity in the pair's central direction immediately before and after the collision, and

$$\bar{f}_{in} = \frac{1}{\delta t} \int_{t^*}^{t^* + \delta t} \left(\mathbf{f}_i^{env} + \mathbf{f}_i^{bond} + \sum_{k \neq j} \mathbf{f}_{ik}^{con} + \mathbf{f}_i^{fric} \right) \cdot \mathbf{n}_{ij} dt \tag{16}$$

is the (averaged) resultant force that act on particle i during the collision in the pair's central direction as a result of all other forces that act on i except for the pair's contact force itself. The post-collision velocity $v_{in}(t^* + \delta t)$ is computed from the coefficient of restitution of the colliding pair (APPENDIX), which must be known a priori. One important aspect in this model is that, when solving the system's dynamics by a time discretization/integration scheme, one finds that the adopted time steps Δt are typically much larger than the collision duration. This requires one to 'smear out' the contact forces over the whole time step, by multiplying them by a factor $\delta t/\Delta t$. Additionally, the value of δt is usually not known and must be arbitrarily chosen for the forces to be computed. A typical choice is $\delta t = \gamma \Delta t$, with $\gamma = 0.01$ (normally, the model is insensitive to γ below 0.01, as reported in [15]).

For the forces due to friction, which arise from the contacts/collisions, we assume by construction that the friction coefficients are small enough so that a continuous slide, with an opposing dynamic friction force, is to be expected between the contacting pair during the entire duration of the contact/collision (Figure 2). In other words, no stick is allowed to occur between the pair. Stick-slip and other more elaborate friction models can be incorporated at little expense, but we find them unnecessary because the friction coefficients are taken here as sufficiently small. Thereby, here we write

$$\begin{aligned} \mathbf{f}_i^{fric} &= \sum_{j=1}^{N_c} \mathbf{f}_{ij}^{fric}, \\ \mathbf{f}_{ij}^{fric} &= \mu_d \left\| \mathbf{f}_{ij}^{con} \right\| \boldsymbol{\tau}_{ij} \quad (\text{continuous slide model}), \end{aligned} \tag{17}$$

where \mathbf{f}_{ij}^{fric} is the (binary) friction force that acts between particle i and particle j , μ_d is the coefficient of dynamic friction for the colliding pair, and

$$\boldsymbol{\tau}_{ij} = \frac{\mathbf{v}_{jt} - \mathbf{v}_{it}}{\left\| \mathbf{v}_{jt} - \mathbf{v}_{it} \right\|} \tag{18}$$

is the tangential direction of the contact/collision, which is the direction of the tangential relative velocity, computed as earlier with

$$\begin{aligned} \mathbf{v}_{it} &= \mathbf{v}_i - (\mathbf{v}_i \cdot \mathbf{n}_{ij}) \mathbf{n}_{ij} \\ \mathbf{v}_{jt} &= \mathbf{v}_j - (\mathbf{v}_j \cdot \mathbf{n}_{ij}) \mathbf{n}_{ij}. \end{aligned} \quad (19)$$

3. MODELING OF THE CELL MEMBRANE AND ITS LIPID BONDINGS

We consider a two-dimensional, circular-shaped idealization of the cell membrane, as depicted in Figure 3 (a fully three-dimensional one can be considered without any modification, at the only expense of having more particles in the system). We neglect, for simplicity, the presence of other substances (proteins, sugars, cholesterol, etc.) rather than lipids on the membrane surface. Within this setting, we assume that each lipid molecule is represented by a spherical particle (corresponding to the molecule's headgroup) that is bonded to its neighboring ones of the same layer by means of SDs, as indicated in the upper zoom of Figure 3.

To capture the 'through-the-thickness' or 'transverse' bonding that maintains the two layers together (which is in great part due to hydrophilic/hydrophobic interactions with the surrounding aqueous media), we assume that there exist transversal SDs connecting the particles in the membrane's radial direction. And to account for circumferential interactions between the two layers, crosswise SDs are introduced. The scheme is as depicted in the lower zoom of Figure 3, where the dashpots are not shown for the sake of clarity. Each SD is taken with stiffness k_{bond} , damping constant c_{bond} , and initial length L_0 . It is important to notice the role of the crosswise SDs. They can be understood as arising from the small lateral interactions that exist between hydrocarbon chains of adjacent lipid molecules. Their presence is crucial in providing a combined bending behavior for the two layers. Not having them causes each layer to deform as independent sheets upon bending, which is not what is observed in real cell membranes.

With such a scheme, on each particle i of the membrane, there act five bonding forces, corresponding to the five SDs that are connected to it. This allows us to write, for each of these particles,

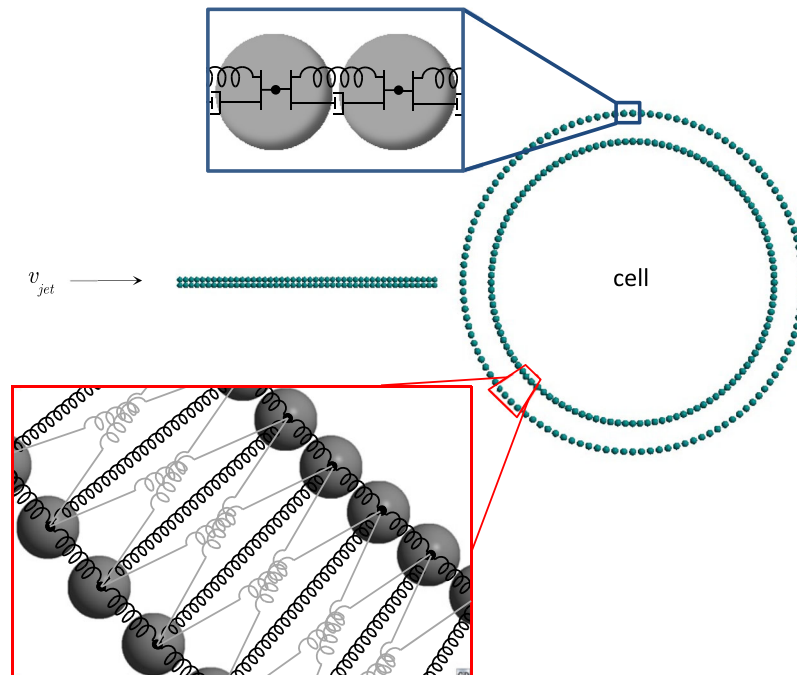


Figure 3. Two-dimensional representation of the cell membrane and bonding between lipid particles.

$$\begin{aligned} \mathbf{f}_i^{bond} &= \sum_{j=1}^5 \mathbf{f}_{ij}^{bond}, \\ \mathbf{f}_{ij}^{bond} &= k_{bond} \Delta L \mathbf{n}_{ij} - c_{bond} (v_{in} - v_{jn}) \mathbf{n}_{ij}, \end{aligned} \quad (20)$$

where

$$\Delta L = \|\mathbf{r}_i - \mathbf{r}_j\| - L_0 \quad (21)$$

is the elongation of the spring that connects the pair $\{i, j\}$ and

$$v_{in} = \mathbf{v}_i \cdot \mathbf{n}_{ij} \quad \text{and} \quad v_{jn} = \mathbf{v}_j \cdot \mathbf{n}_{ij} \quad (22)$$

are the central components of the pair's velocities \mathbf{v}_i and \mathbf{v}_j , respectively. To allow for the bonds to break (rupture) if the particles are pulled apart strongly enough, we provide each SD with a critical strain ε_{crit} that leads to a critical elongation ΔL_{crit} . Once this critical value is reached, the corresponding SD is turned off, that is, it does not enter the summation in Equation (20).

One important issue in this model is how to come up with appropriate values for the springs' stiffnesses. We suggest that they be estimated from surface tension or surface energy arguments, because the value of the surface tension (or interfacial free energy per unit area) for hydrocarbon–water interfaces is well documented in the literature. This is reported as being around 50 mJ/m² for monolayers (although the presence of the hydrophilic headgroup may reduce it to something closer to 20 mJ/m², see, e.g., [19]), so that for bilayers, it must be simply multiplied by two. The reader interested on the physics of this topic is referred to [21] and the many works that followed, and also to the comprehensive work in [19]. Another possibility to estimate k_{bond} is to use direct [22] or indirect [23] experimental measures performed on specific types of membranes, whereby membrane deformations are quantified—often involving electron microscopy visualization—and transformed into an elasticity or stiffness constant (a vast amount of literature is also available on this). Or to use continuum models (e.g., a shell-like kinematical description and its finite element discretization) with which the membrane deformation could be studied under simple load conditions and the particle adhesion forces derived by some correlation. Alternatively, as a rough approximation, one could estimate them from the (more or less known) value of the maximum internal pressure that the cell can undergo before membrane rupture. From static equilibrium arguments on one isolated particle, one can equate the force due to this internal pressure to the sum of the components of its spring forces on the radial direction. By assuming that all springs have the same stiffness, k_{bond} follows.

We remark that the approach proposed in this section, that is, the use of SDs to represent bonding forces between particles, can be used in a number of other problems whenever pair-wise adhesion is observed. The only requirement is that the SDs be judiciously placed according to the problem at hand so as to capture the desired bonded motion of the corresponding particles. Also, because in the approach, each individual bonding is assumed to behave according to a one-dimensional constitutive relation, more complex laws such as nonlinear hyperelasticity with progressive damage and rupture (allowing for non-abrupt breaking) can be straightforwardly incorporated (in such cases, estimation of the constitutive parameters is obviously more complicated but not impossible, see, e.g., [24]). The approach also constitutes a very simple way to enforce fixed (predetermined) interacting pairs, because every bonding pair has to be explicitly defined a priori.

Remark 1. The spring stiffness k_{bond} and the dashpot constant c_{bond} can be understood as ‘homogenized’ properties that represent the overall (average) behavior of the intermolecular interactions between two immediate neighboring lipid molecules. In fact, we believe that many of the physical properties of the cell membrane can be qualitatively described without the need to resort to detailed representations of the complex short-range forces that act between the polar headgroups and hydrocarbon chains of its lipid molecules. In an analogy

with gas–liquid phase interactions in thermodynamics, for example, the classical van der Waals equation of state contains no information on the characteristics and range of intermolecular forces and yet renders a very satisfactory representation of the phase behavior.

- Remark 2. The friction coefficient μ_d of Equation (17) can also be interpreted as a homogenized property in this model. In fact, at such small scales as those observed here, one may argue that the particles may not even come into real contact with each other. A particle-based approach in this case should be viewed more like a coarse-grained molecular dynamics model wherein pair-wise interactions are given by contact and friction laws instead of potential expressions. Thus, friction does not necessarily imply physical friction, but rather a model for the tangential part of the complex short-range interactions between the particles. It may be understood as a simple way of enforcing energy dissipation in the tangential direction whenever two particles come close enough to each other, the dissipation parameter of which being the friction coefficient.
- Remark 3. It could be argued that the compressive response of the membrane on its tangential (surface) direction should be enforced to be zero, as in the relaxed theory of perfectly elastic solids (see Pipkin [25] for early mathematical accounts on this theory). This is suggested by many authors when dealing with continuum mechanics models for thin elastic membranes. In these cases, Steigmann and coworkers [26, 27] have demonstrated that a necessary condition for the existence of energy minimizers is that the structural members carry no load in compression. While this assumption could be readily incorporated into our model (by enforcing $k_{bond}=0$ whenever $\Delta L < 0$ in Equation (20)), here instead we believe that the compressive response should not be neglected. Indeed, one could go even further and improve the model by adopting different values for the compressive and tensile stiffnesses of the bondings. Similarly, different values for the properties of the crosswise springs could be considered.

4. SOLUTION OF SYSTEM'S DYNAMICS VIA NUMERICAL TIME INTEGRATION

To resolve the system dynamics, let us start by considering the acceleration vector of each particle, which may be computed from Equation (3). This vector is related to the particle's velocity by the time-continuous differential equation

$$\frac{dv_i}{dt} = a_i. \quad (23)$$

Integration of this equation between time instants t and $t + \Delta t$, together with Equation (3), furnishes

$$v_i(t + \Delta t) = v_i(t) + \frac{1}{m_i} \int_t^{t+\Delta t} f_i^{tot} dt. \quad (24)$$

The integral in Equation (24) is difficult (if not impossible) to be evaluated analytically because of the intricate dependence of f_i^{tot} with respect to t . A numerical approximation is thus necessary, and here, we adopt the following scheme, which corresponds to the use of a generalized trapezoidal rule:

$$\int_t^{t+\Delta t} f_i^{tot} dt \approx [\phi f_i^{tot}(t + \Delta t) + (1 - \phi) f_i^{tot}(t)] \Delta t, \quad (25)$$

with $0 \leq \phi \leq 1$. If $\phi = 0$, the integration corresponds to an (explicit) forward Euler scheme; if $\phi = 1$, to an (implicit) backward Euler one; and if $\phi = 0.5$, to the (implicit) classical trapezoidal rule. By inserting Equation (25) into Equation (24), one has

$$\mathbf{v}_i(t + \Delta t) = \mathbf{v}_i(t) + \frac{\Delta t}{m_i} [\phi \mathbf{f}_i^{tot}(t + \Delta t) + (1 - \phi) \mathbf{f}_i^{tot}(t)]. \quad (26)$$

On the other hand, the velocity vector of each particle is related to the particle's position by the time-continuous differential equation

$$\frac{d\mathbf{r}_i}{dt} = \mathbf{v}_i. \quad (27)$$

This equation can also be integrated between t and $t + \Delta t$, yielding

$$\mathbf{r}_i(t + \Delta t) = \mathbf{r}_i(t) + \int_t^{t+\Delta t} \mathbf{v}_i dt. \quad (28)$$

The integral on the right side of Equation (28) is also difficult to be evaluated analytically, and then, we adopt the following approximation, similarly to what was performed in Equation (25):

$$\int_t^{t+\Delta t} \mathbf{v}_i dt \approx [\phi \mathbf{v}_i(t + \Delta t) + (1 - \phi) \mathbf{v}_i(t)] \Delta t. \quad (29)$$

By introducing Equation (29) into Equation (28), one arrives at

$$\mathbf{r}_i(t + \Delta t) = \mathbf{r}_i(t) + [\phi \mathbf{v}_i(t + \Delta t) + (1 - \phi) \mathbf{v}_i(t)] \Delta t. \quad (30)$$

Expressions (26) and (30) constitute a set of equations for $i = 1, \dots, N_p$ particles, with which the velocity and position vectors of each particle at $t + \Delta t$ may be computed once $\mathbf{v}_i(t)$ and $\mathbf{r}_i(t)$ are known. This computation, however, cannot be performed directly, because Equation (26) requires the evaluation of $\mathbf{f}_i^{tot}(t + \Delta t)$, which is in turn a function of all (!) unknown position and velocity vectors $\mathbf{r}_j(t + \Delta t)$ and $\mathbf{v}_j(t + \Delta t)$:

$$\begin{aligned} \hat{\mathbf{f}}_i^{tot}(t + \Delta t) &= \hat{\mathbf{f}}_i^{tot}(\mathbf{r}_1(t + \Delta t), \mathbf{r}_2(t + \Delta t), \dots, \mathbf{r}_{N_p}(t + \Delta t), \\ &\quad \mathbf{v}_1(t + \Delta t), \mathbf{v}_2(t + \Delta t), \dots, \mathbf{v}_{N_p}(t + \Delta t)) \\ &= \hat{\mathbf{f}}_i^{tot}(\mathbf{r}_j(t + \Delta t), \mathbf{v}_j(t + \Delta t)), \quad j = 1, 2, \dots, N_p \end{aligned} \quad (31)$$

(the notation with a superposed hat as introduced earlier indicates that the quantity is a function of the arguments inside the parentheses). This fact means that all equations are strongly coupled, and a recursive solution is thereby necessary. We adopt here a fixed-point iterative scheme, whose main steps are as summarized in Equation (32). The scheme is relatively easy to be implemented, and it is noteworthy that no system matrix is required. Moreover, adaptivity of the time step size can be straightforwardly incorporated. One can prove that such kinds of schemes are convergent by realizing that they involve a

GIVEN QUANTITIES : $t = 0$, $\Delta t = \text{known}$, $\phi = \text{known}$, $\mathbf{r}_i(t)$, $\mathbf{v}_i(t) = \text{known}$;

(1) INITIALIZE TIME-STEP :

$K = 0$ (iteration counter)

$\mathbf{r}_i^K(t + \Delta t) = \mathbf{r}_i(t)$, $\mathbf{v}_i^K(t + \Delta t) = \mathbf{v}_i(t)$ (predictor)

(2) FOR $i = 1, \dots, N_p$ DO :

$$\begin{cases} \mathbf{f}_i^{\text{tot},K+1}(t + \Delta t) = \mathbf{f}_i^{\text{tot}}(\mathbf{r}_j^K(t + \Delta t), \mathbf{v}_j^K(t + \Delta t)) \\ \mathbf{v}_i^{K+1}(t + \Delta t) = \mathbf{v}_i(t) + \frac{\Delta t}{m_i} [\phi \mathbf{f}_i^{\text{tot},K+1}(t + \Delta t) + (1 - \phi) \mathbf{f}_i^{\text{tot}}(t)] \\ \mathbf{r}_i^{K+1}(t + \Delta t) = \mathbf{r}_i(t) + [\phi \mathbf{v}_i^{K+1}(t + \Delta t) + (1 - \phi) \mathbf{v}_i(t)] \Delta t \end{cases}$$

(3) CHECK FOR CONVERGENCE :

compute error(\mathbf{r}) and error(\mathbf{v})

IF (error(\mathbf{r}) OR error(\mathbf{v}) > TOL) $\Rightarrow K = K + 1$, GOTO (2) (iterate)

IF (error(\mathbf{r}) AND error(\mathbf{v}) \leq TOL) $\Rightarrow t = t + \Delta t$, GOTO (1) (move to next timestep)

(32)

contraction mapping for all $\mathbf{r}_i^{K+1}(t + \Delta t)$ (K being the iteration counter). Details can be found in [15, 28].

Remark 4. According to Equation (32), velocities and positions seem to be fully updated only after one complete iteration. This would correspond to a Jacobi-type of scheme and is presented like so only for the sake of algebraic simplicity. What we actually do in step (2) of the algorithm is for each particle i , we compute $\mathbf{f}_i^{\text{tot},K+1}(t + \Delta t)$ using the velocities and positions of the previous particles that have just been updated within the current iteration, that is, using $\mathbf{v}_j^{K+1}(t + \Delta t)$ and $\mathbf{r}_j^{K+1}(t + \Delta t)$, $j = 1, 2, \dots, i - 1$. For $j \geq i$, the values of the previous iteration, that is, $\mathbf{v}_j^K(t + \Delta t)$ and $\mathbf{r}_j^K(t + \Delta t)$, are used. This resembles a Gauss–Seidel scheme, which (as it is well known) converges at a faster rate than the Jacobi method, if the Jacobi method converges, or diverges at a faster rate, if the Jacobi method diverges. For details on this subject, the reader is referred to [29].

Remark 5. The two error measures in step (3) of Equation (32) are taken as normalized (nondimensional) measures, and are given respectively by

$$\begin{aligned} \text{error}(\mathbf{r}) &= \frac{\sum_{i=1}^{N_p} \|\mathbf{r}_i^{K+1}(t + \Delta t) - \mathbf{r}_i^K(t + \Delta t)\|}{\sum_{i=1}^{N_p} \|\mathbf{r}_i^{K+1}(t + \Delta t) - \mathbf{r}_i(t)\|} \text{ and} \\ \text{error}(\mathbf{v}) &= \frac{\sum_{i=1}^{N_p} \|\mathbf{v}_i^{K+1}(t + \Delta t) - \mathbf{v}_i^K(t + \Delta t)\|}{\sum_{i=1}^{N_p} \|\mathbf{v}_i^{K+1}(t + \Delta t) - \mathbf{v}_i(t)\|}. \end{aligned} \quad (33)$$

5. NUMERICAL SIMULATIONS

In this section, we provide examples of numerical simulations to show, from a general perspective, how our computational framework can be used to study the delivery of substances into cells. We recall that it is not our intention here to perform thorough assessment of the model's parameters and obtained results but instead just to illustrate how the model works and how it may be applied to the simulation of particle bombardment systems. As previously stated, detailed calibration of parameters and validation against results from physical experiments are left as a matter of further research, which is currently being conducted by the authors and will be presented soon.

As a model problem, we consider the shooting of a single cell by particle jets of different geometrical characteristics and different incoming velocities. We adopt a two-dimensional idealization of the cell identical to the one presented in Section 3, wherein the existence of other materials rather than lipids on the membrane surface is ignored for the sake of simplicity (again, we emphasize that fully three-dimensional models, with embedded particles representing proteins, sugars, cholesterols, etc., can be adopted without any modification, at the only expense of having more particles in the system). The presence of subcellular components in the cell interior is also ignored, as a first approach to the problem. One should keep in mind that such components (especially the actin filament networks) may offer a significant contribution to the mechanical response of the cell. Within the present framework, these networks could be incorporated as chains of particles connected to each other by SDs, being randomly placed in cell cytoplasm.

Two types of cells are considered, both with a perfectly circular initial shape: a ‘small cell’, for which the diameter is taken as $L=100$ nm and a ‘big cell’, for which $L=500$ nm (here we mean ‘big’ only relatively, because cells—even prokaryotic cells—can be bigger than this). The jet is also idealized in a two-dimensional setting, consisting of particles that are regularly distributed over a rectangular area of length 100 nm and width w_{jet} . The problem is as depicted in Figure 4.

We consider different scenarios for each type of cell by varying some of the geometric parameters of the jet: (i) its width is taken either as $w_{jet}=0.02L$ or $w_{jet}=0.1L$, meaning that it is either a ‘thin jet’ or a ‘thick jet’, respectively; and (ii) the diameter of its particles is taken either as $\phi_{jet}=0.5\phi_{lipid}$ or $\phi_{jet}=2\phi_{lipid}$, meaning that it is either a ‘fine-grained’ or a ‘coarse-grained’ jet, respectively. In all cases, the jet’s incoming velocity can take three different values: $v_{jet}=50$ nm/ns, $v_{jet}=100$ nm/ns, and $v_{jet}=150$ nm/ns. The thickness of the membrane and the diameter of the lipid heads are assumed to be the same for both types of cells, and taken as 10 nm and $\phi_{lipid}=2.5$ nm, respectively.

The particles representing the lipid heads are supposed to be soft spheres so that an overlap-based collision scheme (Equations (10–12)) is used. The damping constant d of this scheme is taken following the ideas of [30], which means

$$d = 2\zeta\sqrt{2\sqrt{R^*}E^*m^*\delta^{1/4}}, \tag{34}$$

wherein ζ is the damping rate of the collision, which must be specified, and m^* is the effective mass of the colliding pair, that is,

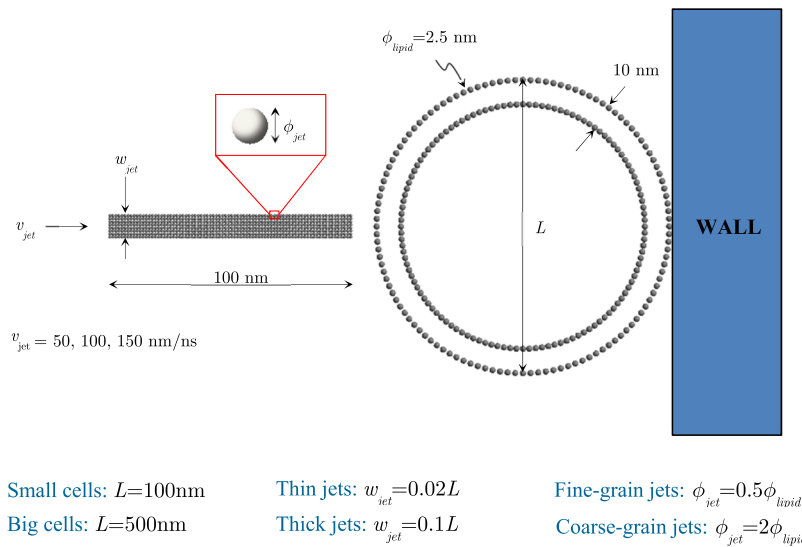


Figure 4. Model problem.

$$m^* = \frac{m_i m_j}{m_i + m_j}. \quad (35)$$

The damping rate ζ enables us to enforce the type of energy dissipation that shall occur during the collision in the pair's central direction. If the colliding pair is seen as one-dimensional SD system (SDS) of mass m^* and damping rate ζ , its dynamics can be fully controlled by specifying appropriate ζ 's. Recalling the solution to a vibration problem of a one-dimensional SDS, it follows that (i) when $\zeta=0$, no damping exists and the collision is a perfectly elastic, energy-conserving one (undamped SDS); (ii) when $0 < \zeta < 1$, small to moderate damping exists and consequently energy dissipation occurs at small to moderate rates (underdamped SDS); (iii) when $\zeta = 1$, strong damping exists and thus rapid energy dissipation is observed (critically damped SDS); and (iv) when $\zeta > 1$, very strong damping with rapid dissipation is observed (overdamped SDS). Equation (34) is a generalization of the ideas proposed by Cundall and Strack [31], wherein only critically damped collisions were considered.

The overlap-based model requires that the collisions be resolved with small time-steps, such that both δ and $\dot{\delta}$ be accurately computed. Here, we use $\Delta t = 0.0002$ ns, chosen so as to ensure at least 5 time steps per collision. This value is arrived at by estimating the duration of a typical collision by means of the Hertz's formula for elastic collisions [20] and then dividing the result by five:

$$duration \cong 2.87 \left(\frac{m^*}{R^* (E^*)^2 v_{rel}} \right)^{1/5} \Rightarrow \Delta t \leq \frac{duration}{5}, \quad (36)$$

where v_{rel} is the relative velocity of the colliding pair in the pair's central direction at the beginning of the collision. The natural frequencies of the bond springs, given approximately by $\sqrt{k_{bond}/m^*}$, must also be checked against Equation (36) in order to avoid poor capturing of the springs vibrations. Such a small time step size leads us to adopt the explicit version ($\phi=0$) of our time integration scheme throughout (an implicit integration would be highly inefficient, because it would perform iterations no matter how small or big Δt is).

As with respect to the cell's surrounding medium, we assume that there exists a pressure gradient from the interior to the exterior of the cell, which leads to an outward pressure force $f_i^{pres} = f_i^p v_i$ on each of the membrane's inner particles (here, f_i^p is the intensity of the force and v_i is the local normal direction of the membrane at the inner particle i , pointing outwards). Direction v_i is computed for each inner particle by taking successive cross-products involving the particle's position vector r_i and its immediate neighboring ones r_{i-1} and r_{i+1} of the internal layer, and then normalizing the result. The pressure force is a live load, in the sense that it changes its direction as the membrane deforms due to the impact of the jet, and therefore each local direction v_i has to be recomputed at every new time step. The intensity f_i^p of this force, however, is kept constant for the sake of simplicity. We assume that particles outside the cell do not experience any pressure forces (but do experience drag).

A rigid wall is placed at the opposite side of the jet to prevent the cell from undergoing large overall rigid body motions when impacted by the jet. The contact of particles with this wall is governed by a damping rate ζ_w and a (dynamic) friction coefficient μ_w . The complete set of data for the problem is as follows:

- mass density of the jet particles = $1000 \text{ kg/m}^3 = 1 \times 10^{-6} \text{ fg/nm}^3$;
- mass density of the cell membrane particles = $900 \text{ kg/m}^3 = 9 \times 10^{-7} \text{ fg/nm}^3$;
- cell internal pressure force magnitude: $f_i^p = 6.5 \times 10^{-5} \text{ nN}$;
- drag force parameters: $c_{env} = 0.000005 \text{ nN} \cdot \text{ns/nm}$ and $v_{env} = \mathbf{o}$;
- spring constant for the bonding forces: $k_{bond} = 5 \times 10^{-3} \text{ nN/nm}$;
- dashpot constant for the bonding forces: $c_{bond} = 0.00001 \text{ nN} \cdot \text{ns/nm}$;
- critical strain for springs rupture: $\varepsilon_{crit} = 0.5$;
- elasticity modulus of jet and membrane particles: $E_{jet} = E_{lipid} = 100 \text{ nN/nm}^2$;

- Poisson coefficient of jet and membrane particles: $v_{jet} = v_{lipid} = 0.25$;
- damping rate for overlap-based collisions: $\zeta = 0.1$;
- coefficient of dynamic friction: $\mu_d = 0.1$;
- gravity is neglected ($\mathbf{g} = \mathbf{o}$);
- initial distance between jet front and cell exterior = 10 nm;

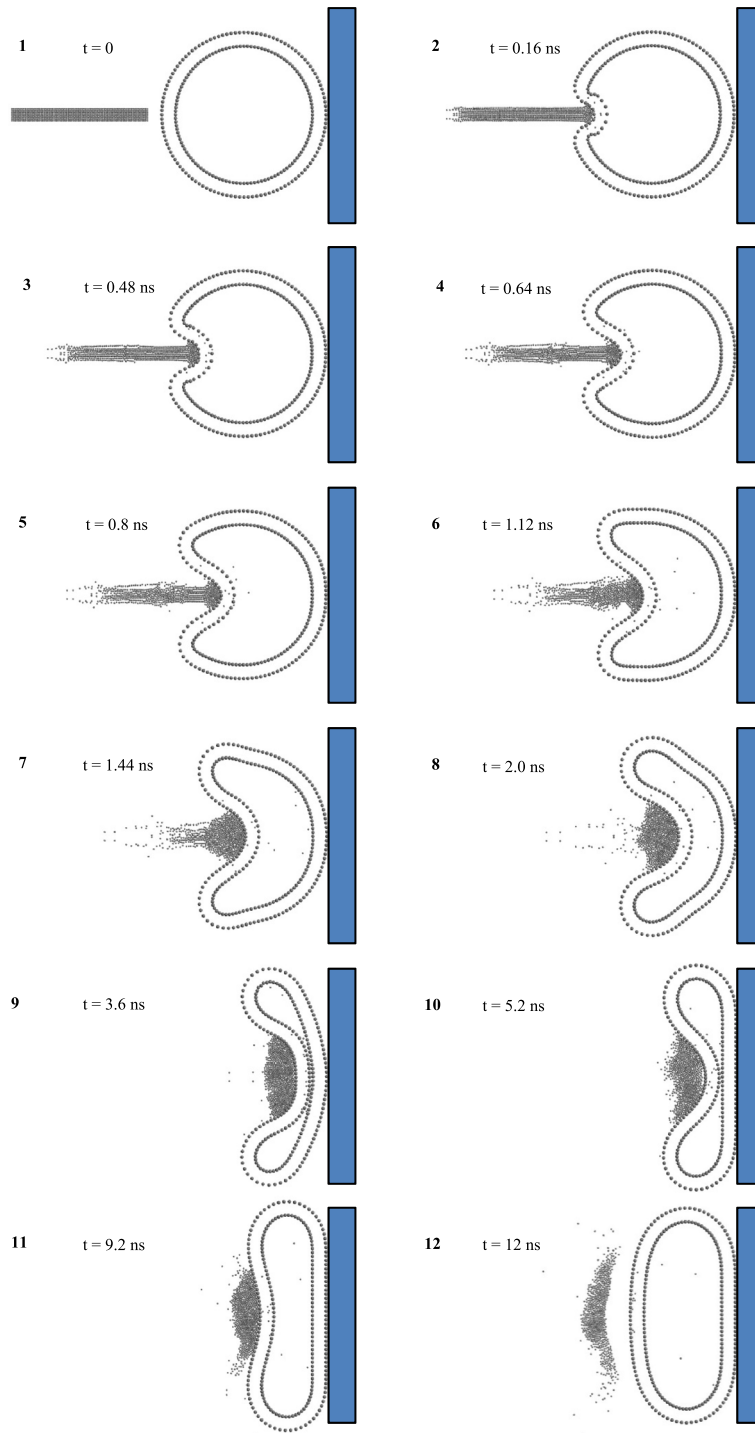


Figure 5. Sequence of snapshots for the small cell bombarded by a thick, fine-grained jet with incoming velocity of 100 nm/ns (sequence is from left to right, top to down).

- rigid wall collision properties: $\zeta_w = 0.1$ and $\mu_w = 0.1$;
- time step size = 0.0002 ns; and
- final time at the end of each simulation = 15 ns.

Figure 5 depicts a sequence of snapshots for a typical simulation, corresponding to the case of the small cell hit by a thick, fine-grained jet at the incoming velocity of $v_{jet} = 100$ nm/ns (this case was chosen arbitrarily just to provide an illustration of how the results can look like in a simulation). Therein, one can see the progression of the membrane deformation with the impact of the jet and

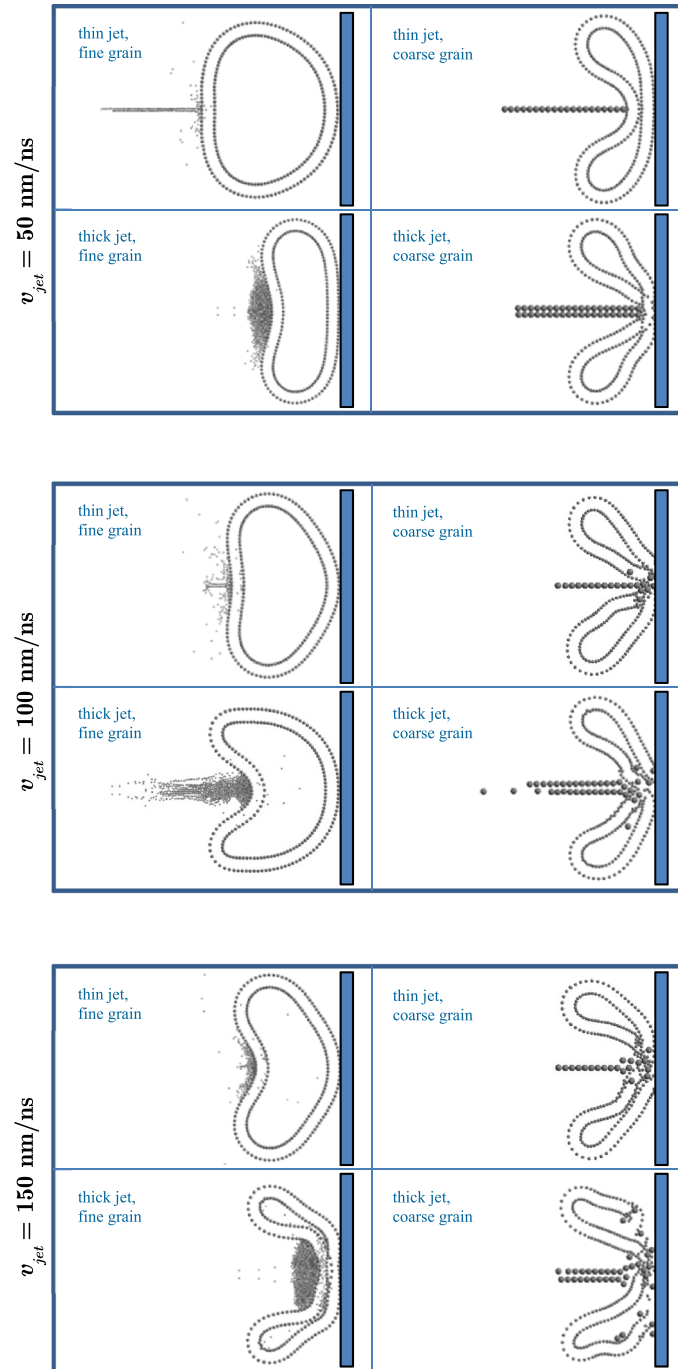


Figure 6. Snapshots of deformed configurations for the small cell when hit by the different kinds of jets at the different incoming velocities.

also the gradual penetration of a few jet particles into the interior of the cell. At the end of the simulation, 12 jet particles (from a total of 640) were observed in the cell's interior. This led to a delivery rate (DR) (defined as the ratio of the number of jet particles inside the cell to the total number of jet particles) of $\sim 1.9\%$. Interestingly, a few particles ended trapped between the two layers of the membrane, what could be a desired effect in some applications. Notice that the cell was able to endure the impact of the jet without experiencing any damage in this case. Moreover, after the jet

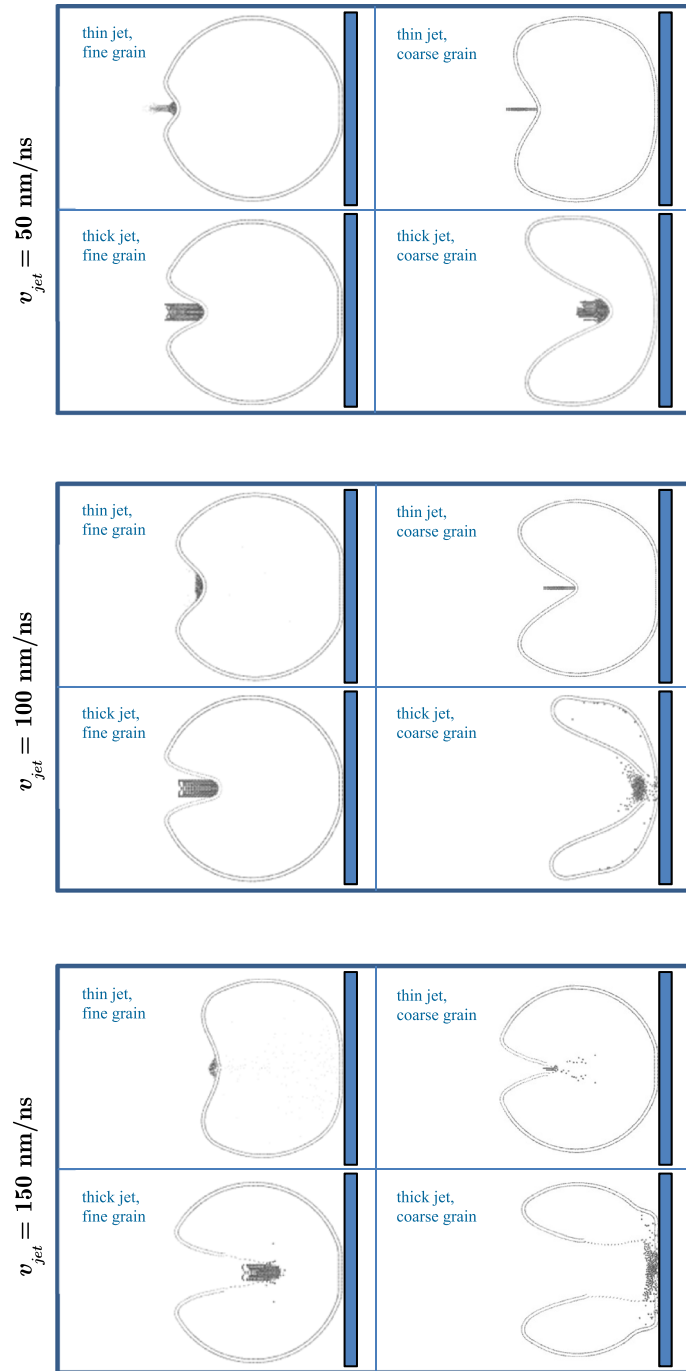


Figure 7. Snapshots of deformed configurations for the big cell when hit by the different kinds of jets at the different incoming velocities.

Table I. Delivery rates (DR) (%) obtained for the model problem.

Jet velocity (nm/ns)		Small cell		Big cell	
		Fine grain	Coarse grain	Fine grain	Coarse grain
50	Thin jet	2.5	0	0	0
	Thick jet	0.3	ED	0	0
100	Thin jet	7.5*	ED	0.9	0
	Thick jet	1.9	ED	4.2	ED
150	Thin jet	12.5	ED	29.0	ED
	Thick jet	11.9	ED	ED	ED

'ED' stands for excessive damage, meaning that the cell breaks into parts due to the impact of the jet.

*All of the delivered particles remained trapped within the two layers of the cell membrane (i.e., none reached the cell cytoplasm).

energy was absorbed (and partly dissipated), the cell tended to recover its initial shape while enclosing the delivered particles within its interior.

In Figure 6, one can see a summary of snapshots, at selected time instants, of the different simulations carried for the small cell (the cell is hit by the different kinds of jets at the different incoming velocities). Figure 7 shows the corresponding results for the case of the big cell. Clearly, the proposed framework can handle multiple contact/impact with opening of localized 'holes' on the membrane, through which the incoming jet particles are occasionally able to pass. This would be very difficult to resolve using other approaches, for example, a continuum (instead of discrete) theory and its accompanying spatial discretization. Table I shows the DRs that resulted from each of these simulations. One can observe that coarse-grained jets either do not penetrate the cells or penetrate but cause excessive damage to the membrane (causing the cell to break into parts). Similarly, jets with the lower incoming velocity (50 nm/ns) display a very poor performance in the delivery. On the other hand, thin, fine-grained jets with the highest incoming velocity (150 nm/ns) deliver the greatest amount of particles to the interior of the cells, and at remarkably high DRs.

It is interesting to observe that, in some of the simulations, a physical (intermolecular) interaction is expected to occur among membrane particles that were not paired (i.e., not connected by SDs) at the beginning of the simulation. This happens, for example, in Figure 5, $t=3.6$ ns and $t=5.2$ ns. Such interaction, however, is of very little magnitude when compared to the contact/collision forces that arise in these particles from the impact by the jet at the adopted jet velocities.

6. CLOSING REMARKS AND FUTURE WORK

The main purpose of this work was to present a simple, yet relatively robust, computational framework to the simulation of the delivery of substances into cells. It is grounded on a particle-based (discrete element) method and can be numerically implemented with small effort by researchers interested in the field. The main advantages of such an approach are that the overall (collective) behavior of the system can be qualitatively represented with little computational cost, and multiple contact/impact with localized rupture is straightforward to characterize. It offers a good picture of the structure and of the dynamics of the cell membrane when it is hit by particles or jets of particles, without requiring detailed descriptions of the complex short-range forces that are present due to intermolecular interactions.

We remark that our intention here was simply to show how the approach works from a general perspective. An in-depth calibration of its parameters and validation against results from physical experiments were left as a matter of further (ongoing) research. Moreover, it is evident that for specific applications, more specific features have to be incorporated, and more specific data need to be considered for both geometrical and material properties. For example, one can render the presence of electric charges relevant to a certain problem and then incorporate near-field forces of the type of Coulombic electrostatic interactions, by adding the term

$$\mathbf{f}_i^{nf} = \sum_{j=1, j \neq i}^{N_p} \frac{q_i q_j}{4\pi\epsilon \|\mathbf{r}_i - \mathbf{r}_j\|^2} \mathbf{n}_{ij} \quad (37)$$

to the particle's total force vector (in this case, q_i and q_j are the electric charges of particles i and j and ϵ is the permittivity). Likewise, the presence of external electric and/or magnetic fields may be considered, by taking them as environmental effects and adding the contributions $q_i \mathbf{E}$ (\mathbf{E} = electric field) and $q_i \mathbf{v}_i \times \mathbf{B}$ (\mathbf{B} = magnetic field) to the particle's environment force vector. These fields can be used to temporarily modify the membrane's mechanical response such that the penetration of incoming particles is facilitated.

In general, coupled multifield approaches are necessary to more realistically simulate biological systems. For example, the deformation response of the membrane can be linked to the concentration s of a certain ion or other chemical species. One can take this into account within our framework by assuming $k_{bond} = \hat{k}(AL, s)$, wherein the evolution of s is described by a differential equation that must also be resolved in the time integration scheme. Or, to allow for gradual (instead of abrupt) rupture of the lipid bondings, a damage model can be coupled to the bonding law. This can encompass a scalar damage variable α , $0 \leq \alpha \leq 1$, such that for a totally undamaged bonding one has $\alpha = 1$, whereas for a totally damaged one $\alpha = 0$. The evolution of α with respect to the spring elongation has to be described by some given law (one possible simple representation is as proposed by [24] for fibrous biological tissues). Thermal effects may also be studied once a multifield solution strategy is implemented.

One important aspect is the identification of parameters that force the system to follow certain desired overall responses. Numerical simulations of the type that is being proposed here can be used to devise inverse problems whereby parameters of particle guns may be obtained by minimizing an appropriate objective function. This can be used to guide or lessen time-consuming laboratory tests. Design-vectors for such objective functions can be consisted, for example, of the following system variables: jet velocity, jet particles' diameter, jet particles' masses, jet-width-to-cell-diameter ratio, jet and/or membrane electric charges, and so on. Because these minimization problems are generally nonconvex, their solutions have to be carried out in a two-stage approach, in which (i) nonderivative algorithms (such as evolutionary genetic algorithms) are used to determine optimal regions in the parameter space and (ii) classical gradient-based schemes are employed in these (locally convex) regions. Such approaches have been used in the context of particulate systems in the works of [32–34]. Uncertainty quantification and design evaluation of input parameters may also be conducted, for example, as recently performed by the authors in [35].

As future steps to the current work, in addition to the ongoing calibration and validation, we may mention (i) post-processing of more detailed statistical information (definition of figures of merit and computation of the various moments), (ii) development of more elaborate constitutive laws for the bonding forces, (iii) incorporation of slightly disordered arrangements for the membrane particles and/or jet particles (perhaps with random perturbations), (iv) consideration of other membrane substances and also of cell internal (cytoplasmatic) material, and (v) formulation of a coupled (multifield) time integration scheme to account for the aforementioned chemical and possibly thermal effects, and also to allow for a more realistic representation of the surrounding fluid (fully coupled fluid-particle interaction). We believe that particle-based models can be a very useful approach to study the delivery of substances across cell membranes, helping advance the design of particle-gun delivery systems.

APPENDIX

For two colliding particles i and j , a balance of linear momentum in the particles' central direction relating the states immediately before (time instant t^*) and after (time instant $t^* + \delta t$) impact renders

$$\begin{aligned} m_i v_{in}(t^*) + m_j v_{jn}(t^*) + \int_{t^*}^{t^* + \delta t} \mathbf{f}_i \cdot \mathbf{n}_{ij} dt + \int_{t^*}^{t^* + \delta t} \mathbf{f}_j \cdot \mathbf{n}_{ij} dt \\ = m_i v_{in}(t^* + \delta t) + m_j v_{jn}(t^* + \delta t), \end{aligned} \quad (A.1)$$

in which subscript n denotes component in the direction of \mathbf{n}_{ij} (Equation (15)) and \mathbf{f}_i and \mathbf{f}_j are, respectively, the sum of all forces that act on particle i and particle j during the collision except for the pair's contact force itself, that is,

$$\begin{aligned}\mathbf{f}_i &= \mathbf{f}_i^{env} + \mathbf{f}_i^{bond} + \sum_{k \neq j} \mathbf{f}_{ik}^{con} + \mathbf{f}_i^{fric} \quad \text{and} \\ \mathbf{f}_j &= \mathbf{f}_j^{env} + \mathbf{f}_j^{bond} + \sum_{k \neq i} \mathbf{f}_{jk}^{con} + \mathbf{f}_j^{fric}.\end{aligned}\tag{A.2}$$

We can write such a balance for each isolated particle as well, what for particle i leads to

$$m_i v_{in}(t^*) + \int_{t^*}^{t^* + \delta t} \mathbf{f}_i \cdot \mathbf{n}_{ij} dt + \int_{t^*}^{t^* + \delta t} I_n dt = m_i v_{in}(t^* + \delta t),\tag{A.3}$$

where the second integral on the left side of the equation amounts to the total impulse that particle i receives from particle j due to impact in the pair's central direction. The collision event can be decomposed into a compression and a recovery phase, with corresponding durations δt_1 and δt_2 , respectively, such that $\delta t = \delta t_1 + \delta t_2$. In the instant of transition from one phase to the other (i.e., instant $t^* + \delta t_1$), the relative velocity of the particles in the direction of \mathbf{n}_{ij} turns to zero, meaning that the pair attains a common velocity v_{cn} in this direction. Accordingly, Equation (A.3) can be decomposed into each one of these phases, yielding

$$m_i v_{in}(t^*) + \int_{t^*}^{t^* + \delta t_1} \mathbf{f}_i \cdot \mathbf{n}_{ij} dt + \int_{t^*}^{t^* + \delta t_1} I_n dt = m_i v_{cn}\tag{A.4}$$

for the compression phase and

$$m_i v_{cn} + \int_{t^* + \delta t_1}^{t^* + \delta t} \mathbf{f}_i \cdot \mathbf{n}_{ij} dt + \int_{t^* + \delta t_1}^{t^* + \delta t} I_n dt = m_i v_{in}(t^* + \delta t)\tag{A.5}$$

for the recovery phase. Similarly, for particle j , one writes

$$m_j v_{jn}(t^*) + \int_{t^*}^{t^* + \delta t_1} \mathbf{f}_j \cdot \mathbf{n}_{ij} dt - \int_{t^*}^{t^* + \delta t_1} I_n dt = m_j v_{cn}\tag{A.6}$$

and

$$m_j v_{cn} + \int_{t^* + \delta t_1}^{t^* + \delta t} \mathbf{f}_j \cdot \mathbf{n}_{ij} dt - \int_{t^* + \delta t_1}^{t^* + \delta t} I_n dt = m_j v_{jn}(t^* + \delta t).\tag{A.7}$$

Equations (A.4) and (A.5), or equivalently, Equations (A.6) and (A.7), provide a means to compute the impulses that each particle receives from the other in the compression and recovery phases in the pair's central direction. The ratio between these impulses is the coefficient of restitution e of the colliding pair, which is a specified (given) quantity:

$$e = \frac{\int_{t^* + \delta t_1}^{t^* + \delta t} I_n dt}{\int_{t^*}^{t^* + \delta t_1} I_n dt}.\tag{A.8}$$

By inserting Equations (A.4) and (A.5) (or equivalently, Equations (A.6) and (A.7)) into Equation (A.8), one arrives at

$$e = \frac{m_i(v_{in}(t^* + \delta t) - v_{cn}) - I_{f_i}^{rec}}{m_i(v_{cn} - v_{in}(t^*)) - I_{f_i}^{comp}} = \frac{-m_j(v_{jn}(t^* + \delta t) - v_{cn}) + I_{f_j}^{rec}}{-m_j(v_{cn} - v_{jn}(t^*)) + I_{f_j}^{comp}}, \quad (\text{A.9})$$

where

$$\begin{aligned} I_{f_i}^{rec} &= \int_{t^*}^{t^* + \delta t} \mathbf{f}_i \cdot \mathbf{n}_{ij} dt, & I_{f_i}^{comp} &= \int_{t^*}^{t^* + \delta t_1} \mathbf{f}_i \cdot \mathbf{n}_{ij} dt, \\ I_{f_j}^{rec} &= \int_{t^*}^{t^* + \delta t} \mathbf{f}_j \cdot \mathbf{n}_{ij} dt & \text{and} & \quad I_{f_j}^{comp} = \int_{t^*}^{t^* + \delta t_1} \mathbf{f}_j \cdot \mathbf{n}_{ij} dt \end{aligned} \quad (\text{A.10})$$

are the impulses due to \mathbf{f}_i and \mathbf{f}_j in the pair's central direction during the recovery and compressive phases. Because v_{cn} is present on both forms of Equation (A.9), it can be eliminated, leading to

$$e = \frac{v_{jn}(t^* + \delta t) - v_{in}(t^* + \delta t) + \Delta_{ij}^{rec}}{v_{in}(t^*) - v_{jn}(t^*) + \Delta_{ij}^{comp}}, \quad (\text{A.11})$$

in which

$$\Delta_{ij}^{rec} = \frac{1}{m_i} I_{f_i}^{rec} - \frac{1}{m_j} I_{f_j}^{rec} \quad \text{and} \quad \Delta_{ij}^{comp} = \frac{1}{m_i} I_{f_i}^{comp} - \frac{1}{m_j} I_{f_j}^{comp}. \quad (\text{A.12})$$

Equation (A.11) furnishes an expression for $v_{jn}(t^* + \delta t)$, which can in turn be inserted into the pair's equation (A.1). By doing so, and considering the definition of the (averaged) resultant force that acts on particle i during the collision given by Equation (16), and the equivalent definition for the (averaged) resultant force that acts on particle j , the following result is attained:

$$\begin{aligned} v_{in}(t^* + \delta t) &= \frac{m_i v_{in}(t^*) + m_j (v_{jn}(t^*) - e(v_{in}(t^*) - v_{jn}(t^*)))}{m_i + m_j} \\ &\quad + \frac{(\bar{\mathbf{f}}_{in} + \bar{\mathbf{f}}_{jn}) \delta t - m_j (e \Delta_{ij}^{comp} - \Delta_{ij}^{rec})}{m_i + m_j}. \end{aligned} \quad (\text{A.13})$$

Once $v_{in}(t^* + \delta t)$ is known, one can subsequently obtain $v_{jn}(t^* + \delta t)$ via Equation (A.11). Finally, having the post-collision velocities, the total impulse that particle i receives from particle j due to impact in the pair's central direction can be computed with the aid of Equation (A.3) (or its equivalent counterpart for particle j), yielding

$$\int_{t^*}^{t^* + \delta t} I_n dt = m_i (v_{in}(t^* + \delta t) - v_{in}(t^*)) - \int_{t^*}^{t^* + \delta t} \mathbf{f}_i \cdot \mathbf{n}_{ij} dt, \quad (\text{A.14})$$

which leads to the (averaged) impulsive force given by Equation (14).

ACKNOWLEDGEMENTS

This work was supported by Fundação de Amparo à Pesquisa do Estado de São Paulo (FAPESP), under the grant 2012/04009-0 (which made possible a research stay for the first author at the University of California at Berkeley, on a sabbatical leave from the University of São Paulo), and by Conselho Nacional de Desenvolvimento Científico e Tecnológico (CNPq), under the grant 303793/2012-0. Material support and the stimulating discussions in Computational Materials Research Laboratory (CMRL, Department of Mechanical Engineering, UC Berkeley) are also gratefully acknowledged.

REFERENCES

1. Sanford JC, Klein TM, Wolf ED, Allen N. Delivery of substances into cells and tissues using a particle bombardment process. *Particulate Science and Technology: An International Journal* 1987; **5**:27–37.
2. Klein TM, Wolf ED, Wu R, Sanford JC. High-velocity microprojectiles for delivering of nucleic acids into living cells. *Nature* 1987; **327**:70–73.
3. Bicanic N. Discrete element methods. In *Encyclopedia of Computational Mechanics, Volume 1: Fundamentals*, Stein E, de Borst R, Hughes TJR (eds). Chichester: John Wiley & Sons; 2004.
4. Pöschel T, Schwager T. *Computational Granular Dynamics*. Springer: Berlin, 2004.
5. Duran J. *Sands, Powders and Grains: An Introduction to the Physics of Granular Matter*. Springer: New York, 1997.
6. Wang Y, Sigurdsson JK, Brandt E, Atzberger PJ. Dynamic implicit-solvent coarse-grained models of lipid bilayer membranes: fluctuating hydrodynamics thermostat. *Physical Review E* 2013; **88**:023301-1-5.
7. Pastor RW, Venable RM. Molecular and stochastic dynamics simulations of lipid membranes. In *Computer Simulation of Biomolecular Systems: Theoretical and Experimental Applications*, Chap. 2, van Gunsteren WF, Weiner PK, Wilkinson AK (eds). Leiden: Escom Science Publishers; 1993; 443–464.
8. Hac AE, Seeger HM, Fidorra M, Heimburg T. Diffusion in two-component lipid membranes –a fluorescence correlation spectroscopy and Monte Carlo simulation study. *Biophysical Journal* 2005; **88**:317–333.
9. Pastor RW. Molecular dynamics and Monte Carlo simulations of lipid bilayers. *Current Opinion in Structural Biology* 1994; **4**:486–492.
10. Tieleman DP, Marrink SJ, Berendsen HJC. Computer perspective of membranes: molecular dynamics studies of lipid bilayer systems. *Biochimica et Biophysica Acta* 1997; **1331**:235–270.
11. Delemotte L, Tarek M. Molecular dynamics simulations of lipid membrane electroporation. *Journal of Membrane Biology* 2012; **245**(9):531–543.
12. Andoh Y, Okazaki S, Ueoka R. Molecular dynamics study of lipid bilayers modeling the plasma membranes of normal murine thymocytes and leukemic GRSL cells. *Biochimica et Biophysica Acta* 2013; **1828**(4):1259–1270.
13. Khelashvili G, Weinstein H, Harries D. Protein diffusion on charged membranes: a dynamic mean-field model describes time evolution and lipid reorganization. *Biophysical Journal* 2008; **94**:2580–2597.
14. Rangamani P, Agrawal A, Mandadapu KK, Oster G, Steigmann D. Interaction between surface shape and intra-surface viscous flow on lipid membranes. *Biomechanics and Modeling in Mechanobiology* 2013; **12**:833–845.
15. Zohdi TI. *Dynamics of Charged Particulate Systems: Modeling, Theory and Computation*. Springer: New York, 2012.
16. Pijush KK, Cohen IM, Dowling DR. *Fluid Mechanics*. Elsevier: Oxford, 2012.
17. Lennard-Jones JE. On the determination of molecular fields. *Proceedings of the Royal Society of London A* 1924; **106**(738):463–477.
18. Johnson KL, Kendall K, Roberts AD. Surface energy and the contact of elastic solids. *Proceedings of the Royal Society of London A* 1971; **324**:301–313.
19. Israelachvili JN. *Intermolecular and Surface Forces*. Elsevier: Amsterdam, 2011.
20. Johnson KL. *Contact Mechanics*. Cambridge University Press: Cambridge, 1985.
21. Jähnig F. What is the surface tension of a lipid bilayer membrane? *Biophysical Journal* 1996; **71**:1348–1349.
22. Ramachandran A, Anderson TH, Leal LG, Israelachvili JN. Adhesive interactions between vesicles in the strong adhesion limit. *Langmuir* 2011; **27**:59–73.
23. Pavinatto FJ, Pavinatto A, Caseli L, Dos Santos Jr DS, Nobre TM, Zaniquelli MED, Oliveira ON Jr. Interaction of chitosan with cell membrane models at the air-water interface. *Biomacromolec* 2007; **8**:1633–1640.
24. Zohdi TI. A computational framework for network modeling of fibrous biological tissue deformation and rupture. *Computer Methods in Applied Mechanics and Engineering* 2007; **196**:2972–2980.
25. Pipkin AC. The relaxed energy density for isotropic elastic membranes. *IMA Journal of Applied Mathematics* 1986; **36**:297–308.
26. Steigmann DJ. Tension field theory. *Proceedings of the Royal Society of London A* 1990; **429**:141–173.
27. Atai AA, Steigmann DJ. Coupled deformations of elastic curves and surfaces. *International Journal of Solids and Structures* 1998; **35**:1915–1952.
28. Zohdi TI. *Introduction to the Modeling and Simulation of Particulate Flows*. SIAM: Berkeley, 2007.
29. Axelsson A. *Iterative Solution Methods*. Cambridge University Press: Cambridge, 1994.
30. Wellmann C, Wriggers P. A two-scale model of granular materials. *Computer Methods in Applied Mechanics and Engineering* 2012; **205–208**:46–58.
31. Cundall PA, Strack ODL. A discrete numerical model for granular assemblies. *Geotechnical* 1979; **29**:47–65.
32. Zohdi TI. Genetic design of solids possessing a random-particulate microstructure. *Philosophical Transactions of the Royal Society A: Mathematical, Physical & Engineering Sciences* 2003; **361**:1021–1043.
33. Zohdi TI. Constrained inverse formulations in random material design. *Computer Methods in Applied Mechanics and Engineering* 2003; **192**:3179–3194.
34. Zohdi TI, Wriggers P. *Introduction to Computational Micromechanics*. Springer: Berlin, 2008.
35. Campello EMB, Zohdi TI. Design evaluation of a particle bombardment system used to deliver substances into cells (accepted for publication). *Computer Modeling in Engineering & Sciences* 2014.